

PAPER • OPEN ACCESS

## Dynamic Strain Aging Behavior in Dual Phase and Multiphase High Strength Steels

To cite this article: J Hu and K S Raghavan 2018 *IOP Conf. Ser.: Mater. Sci. Eng.* **418** 012001

View the [article online](#) for updates and enhancements.

You may also like

- [The deformation-induced martensite and dynamic strain aging during cyclic deformation in AISI 321](#)  
Meng She, Xiaoshan Liu and Guoqiu He
- [Numerical evidences of universal trap-like aging dynamics](#)  
Chiara Cammarota and Enzo Marinari
- [High-Temperature Aging Behavior of Gd-Doped Ceria](#)  
T. S. Zhang, J. Ma, L. B. Kong et al.



**ECS**  
The  
Electrochemical  
Society  
Advancing solid state &  
electrochemical science & technology

**DISCOVER**  
how sustainability  
intersects with  
electrochemistry & solid  
state science research

# Dynamic Strain Aging Behavior in Dual Phase and Multiphase High Strength Steels

**J Hu, K S Raghavan**

AK Steel Corporation, 6180 Research Way, Middletown, OH 45005, USA

Jun.hu@aksteel.com

**Abstract.** Advanced high strength steels, especially dual and multiphase steels, exhibit interesting dynamic strain aging behavior when subjected to isothermal tests at varying strain rates. In this study, uniaxial tensile testing results are presented for two selected steels over a temperature range from 25 to 200 °C at strain rates from  $5 \times 10^{-4}$  to  $5 \times 10^{-1}$  s<sup>-1</sup>. At different temperature and strain rates, some specimens exhibit substantial dynamic strain aging (DSA) effects including negative rate sensitivity and formation of pronounced Portevin Le-Châtelier (PLC) bands resulting in inhomogeneous material deformation. Implications of DSA on performance consequences are addressed in the paper.

## 1. Introduction

Advanced high strength steels (AHSSs) have been successfully applied to build automotive body structures based on a comprehensive consideration of economy, safety, and light-weighting potential. Dual and multiphase steels are especially favored in the material selection due to their enhanced strength and balanced ductility, which in general supports the conventional cold stamping infrastructure in the automotive industry. However, due to the high strength levels of the AHSSs, the adiabatic heat generated from the plastic deformation of these AHSSs can be substantially higher than that of conventional low carbon steels [1]. Additionally, friction-induced heating during large volume production stamping results in ambient tool temperature that is much higher than the conventionally assumed 'cold' stamping conditions. Pereira and Rolfe [2] have reported that tool temperatures during forming DP780 can reach up to 181 °C [2]. Such high temperatures can trigger the dynamic strain aging (DSA) effect during the plastic deformation of sheet metals, which may cause problems, such as rough surface [3], decreased fatigue life [4], early necking and fracture [5], and tooling damage [6].

Dynamic strain aging is a microscopic mechanism involving the interaction between diffusing solute species in the alloy and mobile dislocations during plastic deformation, especially at high temperatures and low strain rates [7]. DSA typically results in serrated flow stress, work hardening, increased Hall-Petch slope, decreased ductility, and negative strain rate sensitivity [8]. The most commonly (but not always) observed macroscopic manifestation of DSA effect is the formation of Portevin Le-Châtelier (PLC) bands, which were named after the two authors who first systematically studied this phenomenon in the year 1909 on steel and in 1923 on aluminum tensile testing samples [9], even though the true first discoverers could have been one century earlier [10]. Typically activated at higher temperature and lower strain rate, the PLC bands associated with serrated stress-strain curves can be observed in: 1) various mechanical tests, including uniaxial tensile [11], compression [12], torsion [13], and biaxial loading [14-16] tests; 2) both polycrystals and single crystals [7]; and 3) BCC, FCC, and HCP alloys



[7]. There are many tools can be used to investigate the PLC bands [6], such as digital image correlation (DIC), speckle pattern interferometry, laser scanning extensometry, thermography, and acoustic emission.

The objective of the present work is to experimentally investigate the DSA indicators and manifestations of two selected AHSSs in uniaxial tensile tests over a temperature range from 25 to 200 °C at strain rates from  $5 \times 10^{-4}$  to  $5 \times 10^{-1} \text{ s}^{-1}$ . Such combinations of temperature and strain rate are designed to represent the different conditions from the laboratory testing to the actual ‘cold’ stamping environments. To thoroughly research the DSA effects, especially the PLC banding, both DIC and thermography were used in the experiments. The results of this work should demonstrate the significant influence of DSA on the deformation behavior of 1200 MPa UTS dual and multi-phase steels, and highlight the importance of controlling the actual tooling temperature even in the ‘cold’ stamping infrastructure.

## 2. Materials and Testing

Two steel grades with ultimate tensile strength (UTS) 1200 MPa were investigated in this study, including a dual phase (DP) and a multiphase grade (with controlled additions of retained austenite (RA) in the microstructure), coded as DP1200 and RA1200. After being machined and proper cleaned, each ASTM E8 tensile specimen was sprayed with random black-white-speckle paint on one surface for the DIC based strain measurement and purely black paint on the other surface for the infrared camera based thermography. In the tests, the specimens were loaded between two grips in the furnace on an electro-mechanical test frame equipped with a 100 kN load cell as seen in Figure 1. The constant crosshead tensile velocities were set to 0.025, 0.25, 2.5, and 25 mm/s, in other words, the nominal strain rates were about  $5 \times 10^{-4}$ ,  $5 \times 10^{-3}$ ,  $5 \times 10^{-2}$ , and  $5 \times 10^{-1} \text{ s}^{-1}$ . Five testing temperatures (25, 50, 100, 150, and 200 °C) were set in this study.

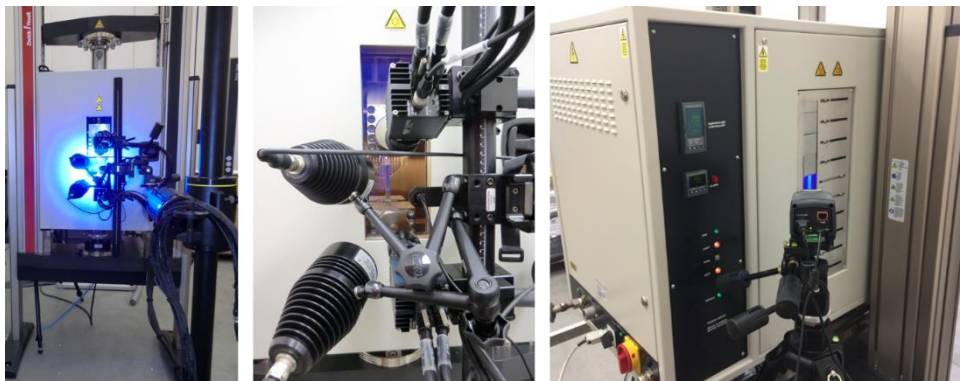


**Figure 1.** The experimental set-up including DIC and infrared camera.

A 3D DIC system was used to in-situ measure the strain field of the specimens through a glass window on the furnace door (Figure 1). Similar set-ups with measurement error analysis have been reported previously in the literature [17]. The DIC system set-up in this study included use of two 4-megapixel CCD cameras operated at frame rates of 1, 10, 100, and 500 fps (corresponding to the four strain rates from slow to fast) to capture the deformation history via a continuous series of  $2358 \times 1728$  pixel<sup>2</sup> photos. The full-field strain evolution were post-processed based on these captured photos in an associated software. The universal load frame and the DIC systems were triggered simultaneously at the beginning of each test, and the crosshead load signals measured in-situ by the load cell were continuously transferred into the DIC software to synchronize with the corresponding photos during the testing. In this way, the stress-strain curves were able to be plotted in the DIC software and accordingly other significant values representing material characteristics could be post-processed.

An infrared thermal camera was used to monitor the temperature field of the specimens through a back-side window on the furnace (Figure 1). This camera can not only show the full-field instantaneous

temperature on the mounted specimens in the furnace but also record the temperature evolution photos ( $640 \times 480 \text{ pixel}^2$ ) during the tests. In this study, both the DIC and the infrared camera were used to evaluate the PLC bands, respectively from standpoints of the strain and temperature fields.

### 3. Results and Discussion

#### 3.1. Strain Rate Effects on Adiabatic Heating

The strain rate of the sheet metal in the actual stamping production is generally recognized as being between  $1\text{--}10 \text{ s}^{-1}$ . In this work, due to the limitation of the load frame and the specimen geometry, the highest strain rate possible was  $0.5 \text{ s}^{-1}$ . Thermography results are shown in Figure 2 for a typical tested specimen including capturing the peak temperature.

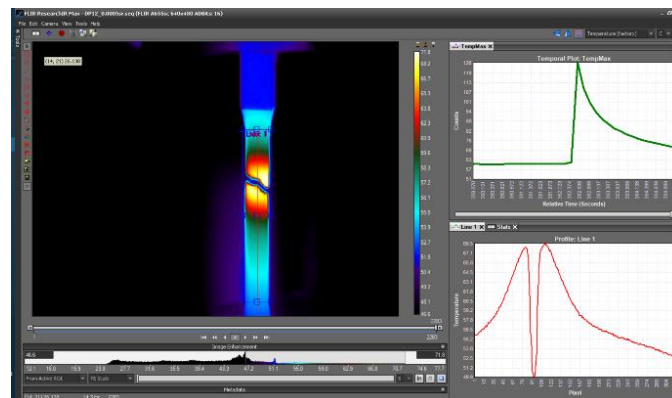


**Figure 2.** Thermographic measurements capturing the peak temperature.

The testing results showing the maximum rise in temperature above ambient condition for the DP1200 and RA1200 specimens are plotted in Figure 3. The most obvious trend noticed was, that the higher the strain rate, the higher the measured temperature rise, independent of ambient temperature used. This is because at higher strain rate, the adiabatic heat has less time to dissipate, and thus accumulates more residual heat on the specimen and induces higher temperature. Moreover, even at  $25 \text{ }^\circ\text{C}$ , the maximum temperatures on the two target grades can rise up to about  $150 \text{ }^\circ\text{C}$  and  $200 \text{ }^\circ\text{C}$  at the highest strain rate, which further implies that the actual stamping temperature can be much higher than conventionally assumed ‘cold’ temperature. It can also be noted that at higher ambient temperatures ( $150$  and  $200 \text{ }^\circ\text{C}$ ) that the adiabatic temperature rise is lower, presumably because of thermal softening of the material leading to less heat generation.

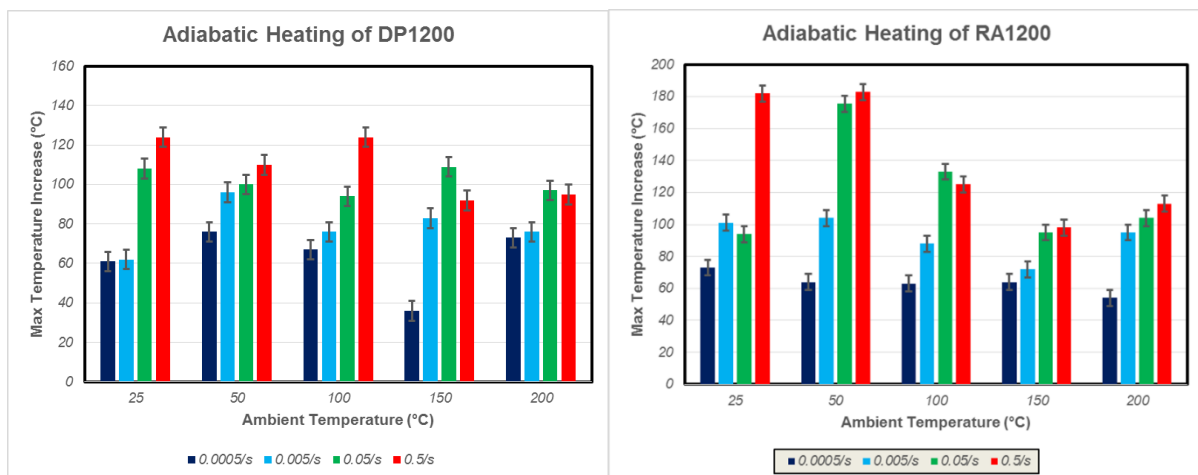


**Figure 3.** Maximum temperature increase on the DP1200 and RA1200 specimens.

### 3.2. DSA Indicators and Effects

As noted in the previous section adiabatic heating may cause sheet metal deformation to happen in the DSA region. Two common DSA indicators on the stress-strain curves are the negative strain rate sensitivity and the serrations (a manifestation of the PLC banding), which, however, need not necessarily occur together. For example, as shown in Figure 4, at 150 °C, the negative strain rate sensitivity can be clearly observed on the stress-strain curves (the higher strain rate, the lower tensile strength) of DP1200, while no serrations appeared. As a comparison, at 200 °C on the same material, both the indicators show up on the stress-strain curves.

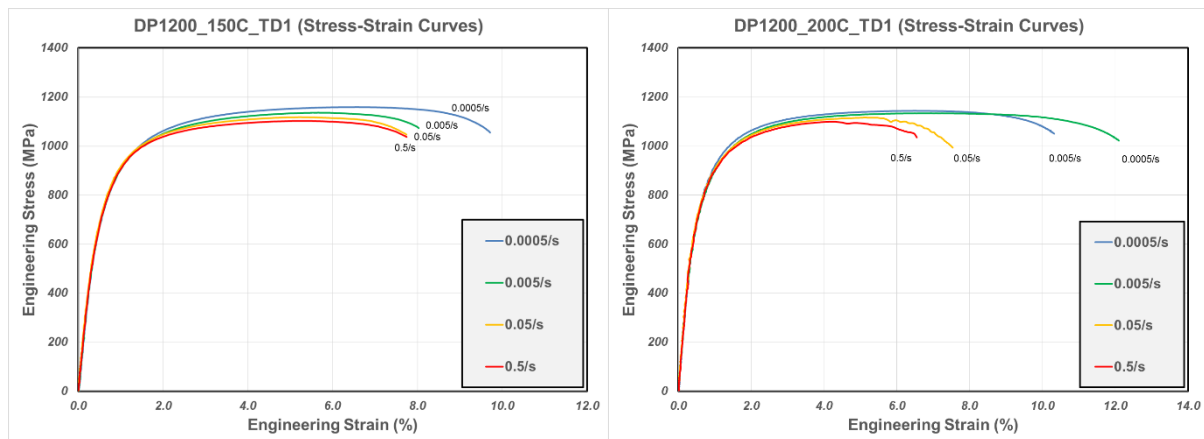


**Figure 4.** Two common DSA indicators: the strain rate sensitivity and the serrations.

Based on these two indicators, the DSA activation maps of the two selected AHSSs can be revealed in the strain rate-temperature diagrams as shown in Figure 5. Compared with the DP1200, the earlier activation of the DSA in RA1200 is possibly due to the higher carbon content in the microstructure, which was used to retain the austenite in the RA1200 producing process [18]. According to the ‘arrested model’ [19], more C-atoms in the microstructure indicate easier ‘dislocation arresting’ during the material deformation. In addition, the diagrams also demonstrate the tendency that the higher temperature and/or lower strain rate, the more likely the DSA will be activated.

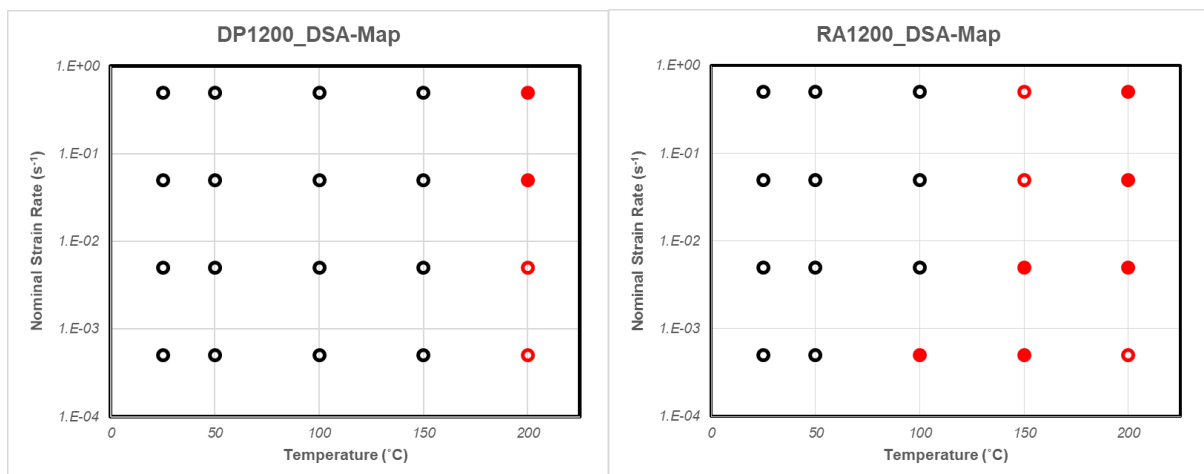


**Figure 5.** The DSA activation maps of DP1200 (left) and RA1200 (right): the black hollow circle shows the DSA-free conditions, the red hollow circle means the DSA region with only the negative strain rate

sensitivity, and the red solid circle indicates the DSA region with both the negative strain rate sensitivity and the serrated stress-strain curves.

The effect of DSA on the material tensile properties should result in improved strength and lower ductility [8]. For both the DP1200 and RA1200, it is observed that with increasing temperature, mobility of solute atoms and dislocations is enhanced leading to decreased strength and improved ductility (Figure 6). Furthermore, for the RA1200, which relies on transformation-induced plasticity (TRIP) effect for strengthening, stability of the retained austenite is likely to be sensitive to the temperature [20], and therefore the tensile properties could shift substantially.

Ultimate tensile strength and total elongation are presented for both the selected grades in Figure 6 as a function of temperature and strain rate. For the DP1200, DSA is observed at 200 °C and to some extent suppresses the ductility (especially at 0.5 s<sup>-1</sup>) but did not improve the strength. As for the RA1200, the valley of both strength and ductility between 100 and 150 °C can be explained as the combined consequences of the deactivated TRIP effects and the activated DSA effects. After the valley, however, at 200 °C both the strength and ductility re-rose (especially the 0.0005 s<sup>-1</sup>) indicate the possible re-activated TRIP effects overcoming the DSA effects. Similar experimental results can be found in [1] and [20] on Q&P980 but more work is necessary to better delineate these findings.

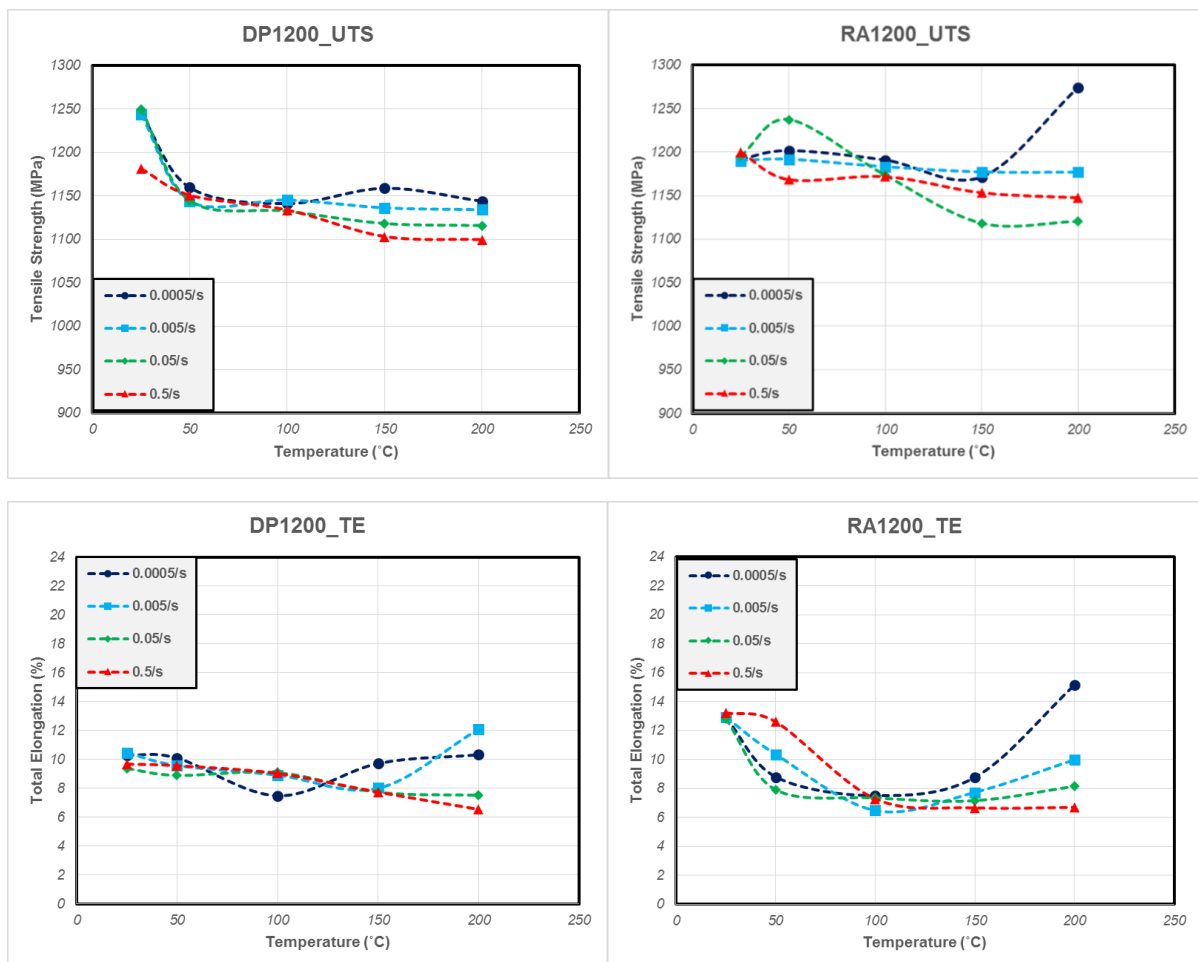


**Figure 6.** The DSA effects on the tensile properties of the DP1200 (left) and the RA1200 (right).

### 3.3. PLC Banding and Appearance

PLC banding is observed in both the thermographic and deformation results. Figure 7 shows the behavior of RA1200 at 200 °C as an example. PLC banding associated with serrated stress-strain curves

can be observed on the specimens tested at 0.005, 0.05, and 0.5  $\text{s}^{-1}$ . At 0.005  $\text{s}^{-1}$ , the apparent serrations showed up on almost the entire range of plastic deformation, while at 0.05 and 0.5  $\text{s}^{-1}$ , the serrations only appeared after the onset of diffuse necking beyond the UTS. Based on the ‘arrested model’ [19], this is because the 200 °C external heat is high enough to provide enough energy for the interstitial atoms (such as C and N atoms) to diffuse, catch up, and ‘arrest’ the moving dislocations only at 0.005  $\text{s}^{-1}$  in the early stage of the deformation; yet in the cases at 0.05 and 0.5  $\text{s}^{-1}$ , only after necking, the decelerated dislocations in the strain localization area can be caught up by the interstitial atoms.

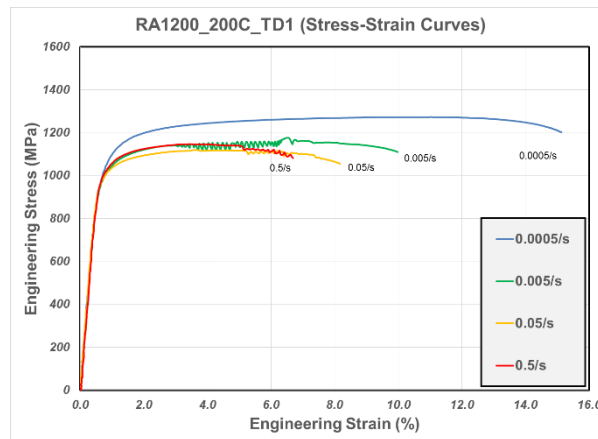


**Figure 7.** The stress-strain curves of RA1200 at 200 °C exhibit both serrated flow stress and negative strain rate sensitivity.

Figure 8 shows detailed serrated flow stress of the RA1200 behavior at 0.005  $\text{s}^{-1}$ . Corresponding major strain rate, major strain and thermographic maps are presented in Figure 9. At the beginning, a PLC band first generated near the lower end of the specimen at 30.3 second (in the test time) and then moved upwards. At 32.4 second, the band moving to the center of the gauge area presented  $\sim 54.55^\circ$  angle to the tensile axis, localized  $\sim 0.043$  more strain, and elevated  $\sim 10^\circ\text{C}$  higher temperature than other regions. Then it disappeared at 38.4 seconds into the upper end. In this period, the flow stress exhibited high-frequency oscillations in Figure 8. After 38.4 second, a new band appeared near the upper end of the gauge area and just kept switching orientation between the backslash- ‘\’ and slash- ‘/’ like shear bands without moving, until final fracture at the same location.

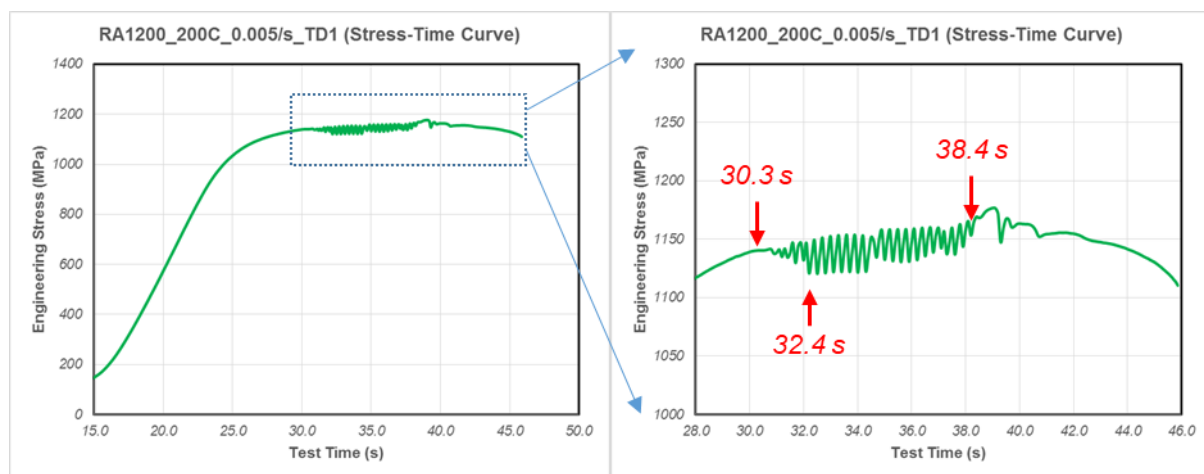


**Figure 8.** Serrated flow stress curve of RA1200 at 200 °C, 0.005  $\text{s}^{-1}$ .

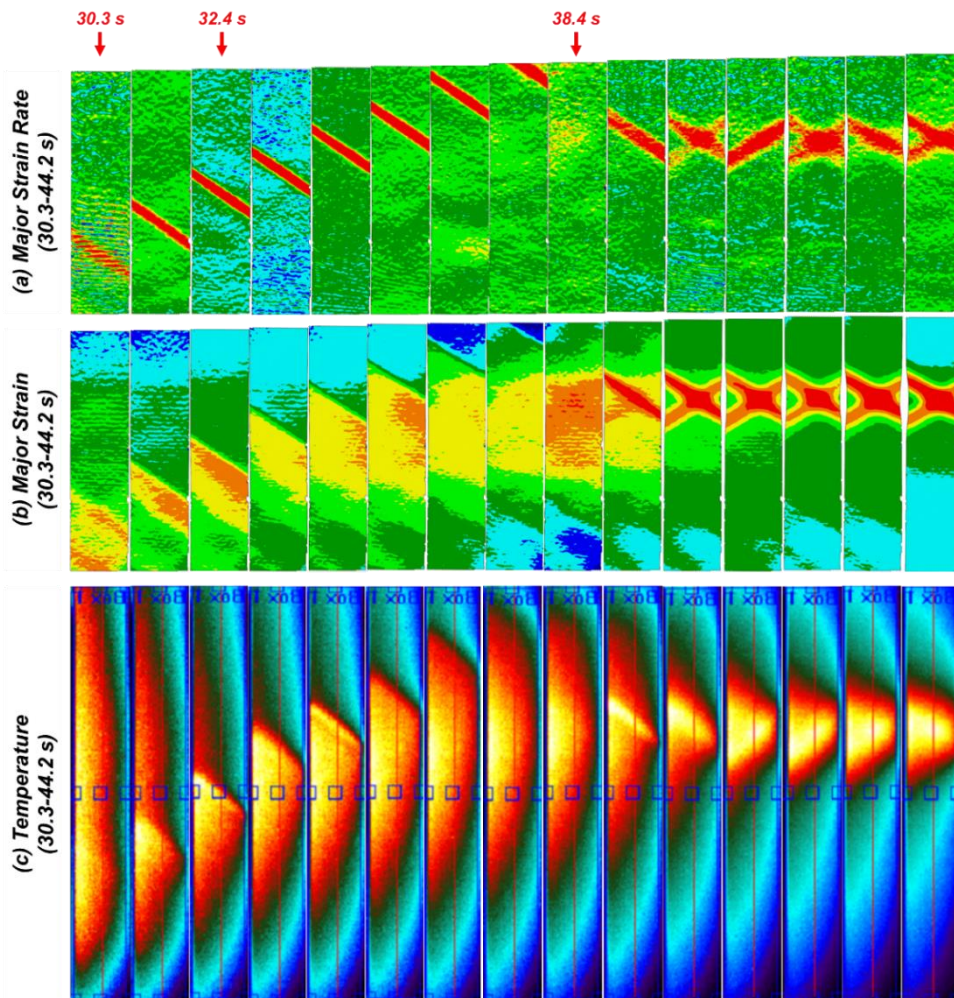


**Figure 9.** PLC bands evolution in (a) major strain rate, (b) major strain, and (c) thermographic fields.

### 3.4. Dynamic Strain Aging and Performance Consequences

As we noted previously, DSA indicators may include negative strain rate sensitivity and serrated flow which is a manifestation of PLC banding. For example in the RA1200 material, we noted that during isothermal testing at 100 °C below a strain rate of 0.0005/s, DSA indicators include both negative strain rate sensitivity and serrated flow. At 150 °C, both serrated flow and negative rate sensitivity occur below 0.005/s and at higher rates there is no serrated flow but involves negative rate sensitivity. At 200 °C, both indicators are present at a strain rate exceeding 0.005/s. These temperatures of 100-200 °C can occur in room temperature forming as a result of adiabatic heating (Figure 3) in regions of relatively high strain or as a result of tool heating during production stamping and may trigger DSA in the form of PLC bands and/or negative strain rate sensitivity. PLC banding occurrence has been reported to cause unsightly roughening marks on the stamped panel, increase flow stress and reduce ductility, and also impair tool life [3-6]. In the regime of negative rate sensitivity, strain rate hardening will be inhibited resulting in accelerated necking behavior. In the case of multiphase steels with retained austenite, occurrence of DSA may also alter TRIP behavior. Further study is warranted to look more carefully into performance consequences of advanced high strength steels.

#### 4. Conclusions

In this work, the adiabatic heating of two selected grades, DP1200 and RA1200, was first experimentally investigated using an infrared thermal camera. The detailed DSA manifestations, especially negative strain rate sensitivity and PLC banding, were also carefully followed with DIC, thermography and stress-strain characteristics. The main conclusions of this study are summarized below.

1. The DSA can be activated by temperature increasing and/or strain rate decreasing. The strain rate sensitivity and the PLC banding are the two effective indicators, both of which were observed in DP1200 and RA1200 materials.
2. The DSA generally suppresses the ductility while enhancing the flow stress. However, interfered by other factors, such as thermal softening and TRIP effects, the eventual DSA effects on the tensile properties can vary. Active DSA regimes in the temperature range of 100-200 °C were observed in both DP1200 and RA1200 materials at the strain rates (0.0005/s-0.5/s) evaluated in this study.
3. As a key manifestation of the DSA, the PLC banding exhibit serrated flow stress and mobile localization of deformation (strain and strain rate) and temperature in the DIC and thermographic measurements. The PLC bands can occur at different periods of deformation and transform to different appearances, depending on the instantaneous temperature, strain rate, and strain level. In this study, PLC bands were observed at 200 °C for DP1200 and above 100 °C for the RA1200 material.
4. Adiabatic heating in both these materials show temperature rise in the sample of 100-200 °C depending on strain rate in room temperature testing. We would therefore expect DSA occurrence during production stamping in these materials.

#### References

- [1] Hu J. Characterization and Modeling of Deformation, Springback, and Failure in Advanced High Strength Steels (AHSSs): Clemson University; 2016.
- [2] Pereira MP, Rolfe BF. Temperature conditions during 'cold' sheet metal stamping. *Journal of Materials Processing Technology*. 2014;214(8):1749-58.
- [3] Robinson JM, Shaw MP. The influence of specimen geometry on the Portevin-Le Chatelier effect in an Al-Mg alloy. *Materials Science & Engineering A (Structural Materials: Properties, Microstructure and Processing)*. 1992;A159(2):159-65.
- [4] Kim DW, Ryu WS, Hong JH, Choi SK. Effect of nitrogen on high temperature low cycle fatigue behaviors in type 316L stainless steel. *Journal of Nuclear Materials*. 1998;254(2-3):226-33.
- [5] Kang J, Wilkinson DS, Jain M, Embury JD, Beaudoin AJ, Kim S, et al. On the sequence of inhomogeneous deformation processes occurring during tensile deformation of strip cast AA5754. *Acta Materialia*. 2006;54(1):209-18.
- [6] Yilmaz A. The Portevin-le Chatelier effect: a review of experimental findings. *Science and Technology of Advanced Materials*. 2011;12(6):063001 (16 pp.).
- [7] Robinson JM, Shaw MP. Microstructural and mechanical influences on dynamic strain aging phenomena. *International Materials Reviews*. 1994;39(3):113-22.
- [8] Rodriguez P, editor Serrated plastic flow. Discussion Meeting on the Mechanical Behaviour of Materials, 7-9 Feb 1983; 1984; India.
- [9] Portevin A, Le Châtelier F. Tensile tests of alloys undergoing transformation. *Comptes Rendus Hebdomadaires des Seances de l'Academie des Sciences*. 1923;176:507-10.
- [10] Franklin SV, Mertens F, Marder M. Portevin-Le Chatelier effect. *Physical Review E (Statistical Physics, Plasmas, Fluids, and Related Interdisciplinary Topics)*. 2000;62(6):8195-206.
- [11] Benallal A, Berstad T, Brvik T, Hopperstad OS, Koutiri I, de Codes RN. An experimental and numerical investigation of the behaviour of AA5083 aluminium alloy in presence of the Portevin-Le Chatelier effect. *International Journal of Plasticity*. 2008;24(10):1916-45.
- [12] Wang J, Guo W-G, Gao X, Su J. The third-type of strain aging and the constitutive modeling of a Q235B steel over a wide range of temperatures and strain rates. *International Journal of*

- Plasticity*. 2015;65:85-107.
- [13] Gilat A, Wu X. Plastic deformation of 1020 steel over a wide range of strain rates and temperatures. *International Journal of Plasticity*. 1997;13(6-7):611-32.
- [14] Swaminathan B, Abuzaid W, Sehitoglu H, Lambros J. Investigation using digital image correlation of Portevin-Le Chatelier Effect in Hastelloy X under thermo-mechanical loading. *International Journal of Plasticity*. 2015;64:177-92.
- [15] Cieslar M, Karimi A, Martin JL, editors. Plastic instabilities during biaxial testing of Al-Fe-Si foils. Aluminium Alloys 2002 Their Physical and Mechanical Properties - ICAA8, 2-5 July 2002; 2002; Switzerland: Trans Tech Publications.
- [16] Romhanji E, Glisic D, Popovic M, Milenkovic V, editors. Stress state effect on dynamic strain aging and surface markings during stretching of AlMg7 alloy sheet. Second Yugoslav Conference on Advanced Materials, 15-19 Sept 1997; 1998; Switzerland: Trans Tech Publications.
- [17] Hu J, Zhang N, Abu-Farha F. Revealing dynamic banding during high temperature deformation of lightweight materials using digital image correlation. Annual Conference on Experimental and Applied Mechanics, 2015, June 8, 2015 - June 11, 2015. Conference Proceedings of the Society for Experimental Mechanics Series. 3. Costa Mesa, CA, United states: Springer New York LLC; 2016. p. 271-9.
- [18] Speer J, Matlock DK, De Cooman BC, Schroth JG. Carbon partitioning into austenite after martensite transformation. *Acta Materialia*. 2003;51(9):2611-22.
- [19] McCormick PG. A model for the Portevin-Le Chatelier effect in substitutional alloys. *Acta Metallurgica*. 1972;20(3):351-4.
- [20] Coryell J, Savic V, Hector L, Mishra S, editors. Temperature effects on the deformation and fracture of a quenched-and-partitioned steel. SAE 2013 World Congress and Exhibition, April 16, 2013 - April 18; 2013 2013; Detroit, MI, United states: SAE International.